

Picosecond Chemical and Biological Events

P. M. Rentzepis

The elementary steps of chemical and biological reactions occur on a time scale between $\sim 10^{-13}$ and 10^{-9} second. It is in this time range that experiments must probe to reveal the fundamentals of reaction kinetics. For example, the primary steps occur in vision when a proton is translocated and in photosynthesis when an electron is transferred from one species to the other, initiating a redox reaction; the bonds broken and formed result in a new species. It is the microchronography of these events that one can view by means of picosecond spectroscopy. Chemical and biological reactions are strongly coupled to vibrational motions that have a frequency of 10^{13} to 10^{10} sec^{-1} , and since most chemical and biological phenomena require at least a few vibrations for their interaction, the

(7), proton transfer reactions (8), solvation of electrons (9), and photosynthesis (10-12). In this article I outline the techniques developed to date and summarize some of the results that have been obtained.

Experimental Techniques

Picosecond spectroscopy had its genesis (1) about 12 years ago, when it became possible to measure easily the time width of light pulses produced by mode-locked lasers through the use of two-photon (13) and three-photon (14) fluorescence methods and direct display on Polaroid film. These methods are still in use, even though it is now possible to use streak cameras instead (15).

Summary. Picosecond spectroscopy is a relatively new field of science that utilizes ultrashort laser pulses to monitor events taking place in the 10^{-12} second regime. The continuing development of picosecond spectroscopy has made possible the detection and measurement of the primary events in many physical and biological processes. This article describes a currently used picosecond spectroscopy system that is capable of reliably recording picosecond events. Two areas of picosecond research are discussed; one concerns the interaction of electrons in fluids, and the second the primary events in vision.

10^{-12} second range becomes the time domain where most of the initial activity takes place and is therefore of most interest to chemists and biologists. The desire to penetrate this time domain, investigate chemical mechanisms, and measure the rates of elementary molecular events is the driving force that has made picosecond spectroscopy not just a new technique but a new field of science in a rather short time.

The realization of picosecond spectroscopic methods has provided new information in a variety of areas in chemical physics as well as chemical kinetics, such as vibrational relaxation (1, 2), radiationless transitions (3-6), cage effects

As with conventional spectroscopy, picosecond spectroscopy has found wide applications in both absorption and emission studies, from ultraviolet to infrared wavelengths. For most experiments the system used is similar to the one shown in Fig. 1 (16), with variations such as use of a dye laser for tunable pulses or a CO_2 laser for experiments in the infrared region, rather than a glass or yttrium aluminum garnet (YAG) laser. The source of picosecond pulses in the apparatus shown in Fig. 1 is a Nd^{3+} /glass laser mode-locked by a saturable absorbing dye, such as Kodak dye 9860. This dye has a fast recovery (~ 8 psec) from the bleached state and provides stable mode locking. The output of the laser consists of ~ 100 pulses each with a time width of 5 to 10 psec and a bandwidth of 10 na-

nometers. The interpulse separation, determined by the length of the cavity, is typically 10 nanoseconds. Although most lasers can be mode-locked for picosecond pulse emission, the highest powers have been achieved with Nd^{3+} /glass, and therefore this system has been used extensively for picosecond experiments.

At present, it is possible to generate short pulses with almost every type of laser. However, the time width, wavelength bandwidth ($\Delta\nu$), and power of laser-generated pulses vary drastically with the oscillating medium and method of pulse generation. Some of the most widely used sources of picosecond pulses include the Nd^{3+} /glass laser because it can generate pulses 4 to 8 psec in duration and can provide several joules of energy in a 50 cm^{-1} bandwidth. A Nd^{3+} /YAG laser may generate equally intense pulses; however, their time width is ~ 20 psec at a $\Delta\nu$ of 0.3 cm^{-1} . Dye lasers, when mode-locked, emit picosecond pulses and have the advantage of tunability over the visible range, but they produce less power than the solid-state laser. It has recently been reported (17) that a rhodamine 6G laser, pumped by an argon laser, emits subpicosecond pulses with an energy of 10^{-9} joule.

Any of the lasers mentioned above provide adequate time resolution to monitor the primary events that govern most fundamental molecular processes in nature. However, for an in-depth study of these effects, one also requires an experimental system that contains at least (i) a picosecond time clock, (ii) a broadband continuum for interrogating spectral changes, and (iii) a sensitive and reliable detection, data-processing, and display system. Such a prototype system is shown schematically in Fig. 1. Following a brief description of these basic components, we will turn to examples where picosecond spectroscopy has provided data essential to conclusions about a number of fundamental molecular processes. It has been shown that a single pulse from an Nd^{3+} /glass laser has a sufficiently high photon content to allow its conversion to second (530 nm), third (355 nm), and fourth (265 nm) harmonics, as well as stimulated Stokes and anti-Stokes pulses that are intense enough to be used for the excitation of molecular species and the generation of interrogating continua covering an even broader spectral range. A single pulse, as shown in Fig. 2, can be well characterized in shape, time width, and bandwidth. The availability of a range of frequencies and high power and the capability of accurately characterizing the

The author is head of Physical and Inorganic Chemistry, Bell Laboratories, Murray Hill, New Jersey 07974.

shape, time width, and bandwidth of a single pulse are often of crucial importance in the interpretation of spectral measurements. Although the rhodamine dye laser apparently provides pulses of subpicosecond duration, experimental subtleties resulting from the need to average over many excitations, as well as the need to excite and monitor at a single wavelength (615 nm), can result in uncertainties sufficient to affect both data and conclusions. For example, should the single wavelength available fall at the isosbestic point of two competing processes, as was the case with bacteriorhodopsin (18), or should there be repetitive pumping, as in hemoglobin (19) and other systems (20), one is necessarily led to an erroneous conclusion.

Single-Pulse Extraction and Amplification

The initial single pulse, which after various modifications becomes the means of excitation and interrogation, is extracted from the mode-locked train of pulses by the use of a Pockels cell and cross polarizers, shown in Fig. 1. In this arrangement, as the pulse passes through the first polarizer and the Pockels cell, a portion of it is reflected to a photodiode, which sends an electric impulse onto a driver connected with the Pockels cell and an 8-kilovolt source. Normally, the pulses reaching the second polarizer are rejected and do not enter the amplifier. However, when the intensity of the probes in the train becomes high, the signal sent to the driver is sufficient for breakdown and allows the high voltage to activate the Pockels cell and induce birefringence. The polarization of the pulse passing through the Pockels cell at this time is rotated by 90°, which enables it to pass through the second polarizer. By applying the high voltage for nearly 6 nsec, only one pulse is extracted from a well-defined and selectable position in the pulse train.

For a variety of reasons, most investigators insist on using a single pulse. Most processes being studied have a decay component that is as long as or longer than the interpulse separation in the mode-locked train, or the sample may undergo irreversible changes on irradiation. In addition, the pulse shape, width, and intensity may vary widely, and reliance on the cumulative effect of hundreds of pulses and an average of unknown and fluctuating pulse properties could be problematic. When a single pulse has been extracted, it is possible to achieve double-pass gains of ≥ 100 in an optical amplifier. Gain saturation, optical

component damage, or both occur before gains of this magnitude can be reached when the entire train is passed through an amplifier. Because of the inefficiency of conversion from 1060 to 265 nm, amplification of the pulse is mandatory for studies in the ultraviolet region.

The average spectrum of many pulses is a smooth band, and because of the nonlinear response of the crystal detector the width appears erroneously narrow. Indeed, the single pulse displayed in Fig. 3 reveals that the output of the Nd³⁺/glass laser is often characterized by a band ~ 100 cm⁻¹ wide with many spikes. Such a complex pulse shape, which changes from pulse to pulse, is not suitable for most chemical studies. To eliminate this problem, it has been found highly desirable to pass the pulse through a Nd³⁺/YAG amplifier: the output is a pulse amplified by a factor of 10 and having the inherent time width of the Nd³⁺/glass and the bandwidth of the Nd³⁺/YAG laser—that is, 4 to 6 psec and a bandwidth of 3 cm⁻¹ compared to 0.3

cm⁻¹ for normal YAG emission at 1064 and 1061 nm (21). Pulses before and after amplification through Nd³⁺/YAG are shown in Fig. 2, A and B.

Excitation and Interrogation

As in conventional spectroscopy, picosecond studies require excitation pulses with a wide range of wavelengths and a high energy content to induce observable changes per pulse, and detection may be by either emission or absorption, or preferably both simultaneously, as in the apparatus shown in Fig. 1.

The 1060-nm pulses have found only limited direct usage in spectroscopic experiments. More frequently, the second harmonic frequency at 530 nm is generated by propagation of the infrared pulses through a second harmonic-generating crystal with a nonlinear polarizability. Additional frequency changes in the pulse may be achieved by repeated harmonic generation or nonlinear mixing to

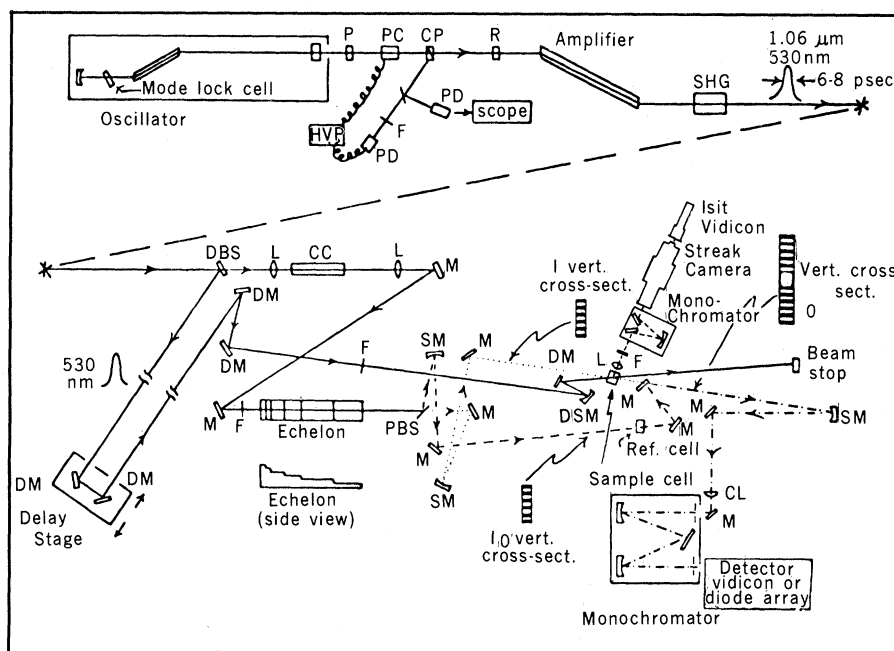


Fig. 1. Apparatus for picosecond spectroscopy with the capability of generating intense picosecond pulses from the near infrared to the ultraviolet and detecting, analyzing, and displaying records of absorption and emission events in the range 10^{-12} to 10^{-6} second. The oscillator is a Nd³⁺/glass or dye laser (21). The amplifier Nd³⁺/YAG or dye laser is pumped with a 530-nm Q-switched pulse (21). The components along the optical path are designated as follows: P, polarizer; PC, Pockels cell; CP, crossed polarizer; PD, photodiode; HVP, high-voltage pulse; R, rotator; SHG, second harmonic-generating crystal; DBS, dielectric beam splitter; CC, continuum cell; DM, dielectric mirror; PBS, pellicle beam splitter; SM, spherical mirror; L, lens; and F, filter. For the train of 1060-nm pulses generated in the Nd³⁺/glass oscillator, a single pulse is extracted by the activated Pockels cell. The pulse is then amplified and sharpened in part of the Nd³⁺/YAG rod and converted to 530 nm. One 530-nm pulse is used for excitation, and the remaining 530-nm and 1060-nm pulses are focused in the continuum cell, dispersed in the echelon into a set of pulses with picosecond separations, and split into a reference beam (I_0) and a probing beam (I) by the PBS. One pulse of the I beam and the excitation pulse are synchronized to arrive simultaneously by means of a delay stage. After the sample cell, beams I and I_0 are imaged onto the slit of a monochromator and then onto a vidicon, which detects the events and transforms the data to digital form for computer processing. The emission is detected by the streak camera and fed to a computer by its ISIT (intensified silicon intensified target) vidicon. This system was constructed and used by Noe *et al.* (45).

obtain the fourth harmonic at 265 nm or the third harmonic at 355 nm; the conversion to higher harmonics has an efficiency of 5 to 25 percent.

Smaller frequency shifts between harmonics may be achieved with high efficiency (~ 10 to 60 percent) by stimulated Raman scattering processes. The magnitude of the shift can be varied from ~ 500 to 4000 cm^{-1} by selecting a molecule with the appropriate Raman transition frequency. Virtually the entire spectral region from near infrared to near ultraviolet is accessible for time-resolved picosecond studies at a coarse resolution of approximately 500 cm^{-1} when both harmonic and Raman-shifted frequencies are used. Recently a tunable picosecond dye laser has been developed that can be used in conjunction with the picosecond laser; it provides for 6-psec, 5-mJ pulses tunable between 380 and 800 nm (22) and can be used for either excitation or interrogation.

Emission and Streak Camera

In the case where the process being studied is monitored by means of its fluorescence or phosphorescence, the apparatus for excitation is the same as shown in Fig. 1. The detector is a spectrometer, with subsequent recording by either a streak camera or a photomultiplier in conjunction with photon-counting equipment. In view of the wide use of photon-counting techniques, which are not specific to picosecond spectroscopy, and the rather restricted employment of streak cameras in spectroscopy, I will describe only briefly the advantages of a streak camera as a detection source of picosecond emission.

The initial proposal for an electro-optical time-resolved photograph of fast luminous events was made in 1956 (23). It was pointed out that the time limit of a streak camera will ultimately be controlled by the transit time of the photoelectron in its image tube. The photoelectron transit time through the tube has a half-width $\Delta t_p = m \Delta V / eE$, where ΔV is the initial electron velocity half-width, e and m are the electron charge and mass, and E is the electric field strength. Since ΔV depends on the illuminating wavelength for any photocathode, the time resolution of a streak camera is ultimately a function of the photocathode type, wavelength, and electric field. Streak cameras are now available that, when coupled to a vidicon, have a time resolution of about 2 psec and a sensitivity approaching that of photon counting. The streak camera has found wide use in

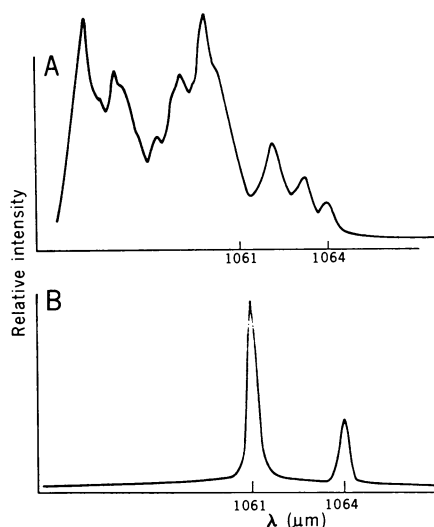


Fig. 2. (A) Spectrum of a Nd^{3+} /glass picosecond pulse. The average spectral width is ~ 100 cm^{-1} . (B) Spectrum of a Nd^{3+} /glass pulse after amplification by a Nd^{3+} /YAG laser. The 1064-nm peak is the well-known Nd^{3+} /YAG laser line. The full width at half-maximum of each of the two amplified picosecond pulses is ~ 3 cm^{-1} and the time width is < 6 psec.

picosecond emission spectroscopy of molecular, biological (24), and chemical (25) systems and as a diagnostic tool for characterizing the picosecond pulse (26). Absorption studies can be performed in which the same pulse is used for excitation and interrogation; however, it is preferable for accuracy and understanding of the process under investigation to employ a monitoring beam with a broad wavelength range.

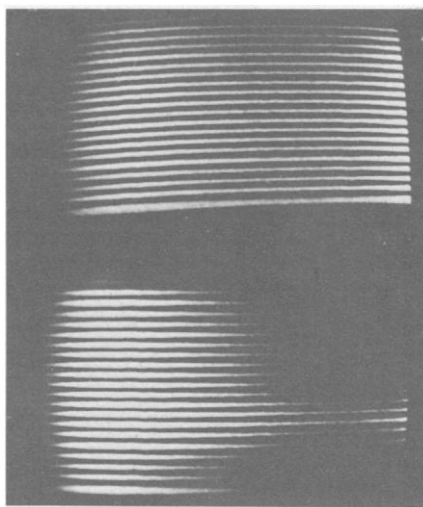


Fig. 3. Time- and frequency-resolved absorbance changes in DODCI caused by an intense 530-nm pulse. The changes were monitored by the continuum light segmented into 6-psec steps by an echelon. Time increased downward and the fourth segment was coincident with the excitation pulse. Bleaching and recovery occurred rapidly, in ~ 10 psec, and nearly simultaneously across the entire absorption band.

Wavelength and Time Measurement

Until recently, most picosecond spectra were obtained in a point-by-point fashion; that is, the monitoring pulse with a bandwidth of a few nanometers was recorded at a particular delay time after excitation. In a typical operation, a histogram at a single wavelength was determined by translating mirrors or prisms between laser shots. Although the pointwise approach is still in use, many laboratories have adapted dispersive methods in preference to the frequency-shifting and time-delaying techniques. In dispersive methods the probe light pulse, which initially has narrow spectral and temporal widths, is spread out in wavelength and time.

With the strong dispersive techniques currently employed, extended spectral and temporal regions can be covered by a single probe pulse, and thus extended time resolution of broad spectral ranges can be recorded after excitation with a single pulse. This capability not only reduces data collection times but also permits the data to be related to the well-defined optical properties of the single pulse—time width, bandwidth, shape, intensity, and so on. The variation of these parameters with position of the pulse within a mode-locked train has already been mentioned, but additional large variations occur for single pulses selected from one laser shot to the next, making it more difficult, if not impossible, to correlate data gathered in a pointwise manner with the true excitation process. The techniques employed for dispersion of the pulse in wavelength in order to generate a picosecond continuum spread over several hundred nanometers, and the conversion of the single interrogation pulse to a set of pulses separated by a preselected interpulse distance of several picoseconds, are described below.

Continuum

Early work with high-power lasers involved studies of nonlinear interactions such as stimulated Raman scattering in liquids and solids and self-broadening processes in liquids, particularly liquids with high Kerr constants; for instance, the pulse was broadened or dispersed in CS_2 to several hundred wave numbers in bandwidth while its short time width was maintained. It was observed (27) that focusing intense picosecond pulses into many solids and liquids produced superbroadened continua, with widths $> 10^4 \text{ cm}^{-1}$. When it was shown (28) that

these continua were also comparable in duration to the picosecond pulses that produced them, it became clear that these "white light" pulses would be very useful for time-resolved spectroscopy.

Echelon

Time resolution of picosecond events has taken three principal forms. The pulse delay method, used as early as 1967 to study the vibrational relaxation of azulene and the bleaching of dyes (*1*), relies on the average of many repetitive

shots and suffers from the problems of sensitivity and pulse parameter stability mentioned above. The streak camera is much preferred to the pulse delay method and is probably the most reliable and accurate means for recording picosecond events in emission. For absorption studies, the echelon technique (*29*) provides discrete dispersion by creating a set of optical paths for different parts of the cross-sectional area of the probe beam, such that each optical path has a different transit time for light.

Typically, the echelon takes the form of a stepped wedge made by a set of mir-

rors (reflection echelon) or by a set of glass or quartz plates in optical contact (transmission echelon). The time information impressed along the cross section of the beam depends on the thickness of the glass plates and the angle of propagation. Interpulse delays from < 4 to > 200 psec can be obtained in practice, depending on the thickness of the step. Figure 1 shows the probe pulse traversing the cell containing the continuum-generating liquid and then passing through an echelon where the time dispersion is imprinted on it. The probe beam now has taken the form of a train

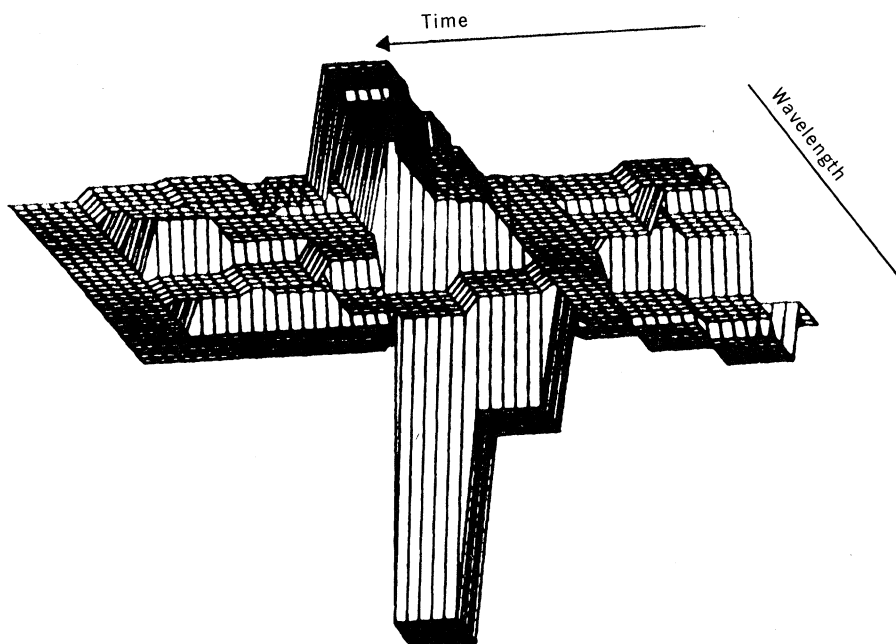
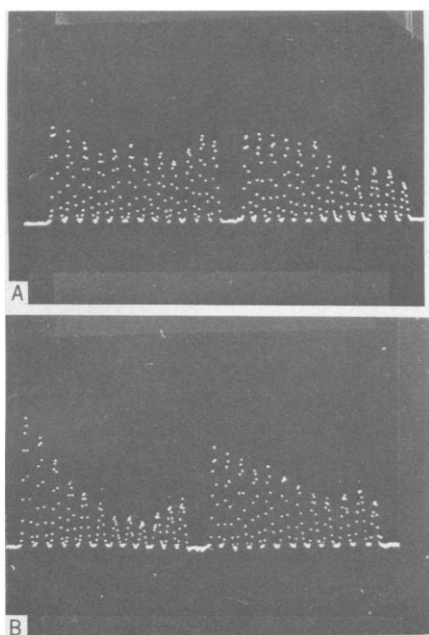


Fig. 4 (left). Output of the vidicon on an optical multichannel analyzer screen. The right side represents the reference beam I_0 and the left side the interrogating beam I . Each segment is 6 psec in duration and is separated from its neighbor by 10 psec. (A) Display of I and I_0 when the excitation beam is blocked from entering the sample cell. (B) Display of I and I_0 after excitation, showing the decreased intensity in the I segments, which indicates that an absorption intermediate is formed. Fig. 5 (right). Three-dimensional display of time (picoseconds), wavelength (nanometers), and absorbance change after excitation with a single 530-nm picosecond pulse. The wavelength range monitored is 550 to 570 nm. The time, in 10-psec segments, covers 100 psec, and the absorbance changes are positive (upward) for absorption and negative (downward) for bleaching.

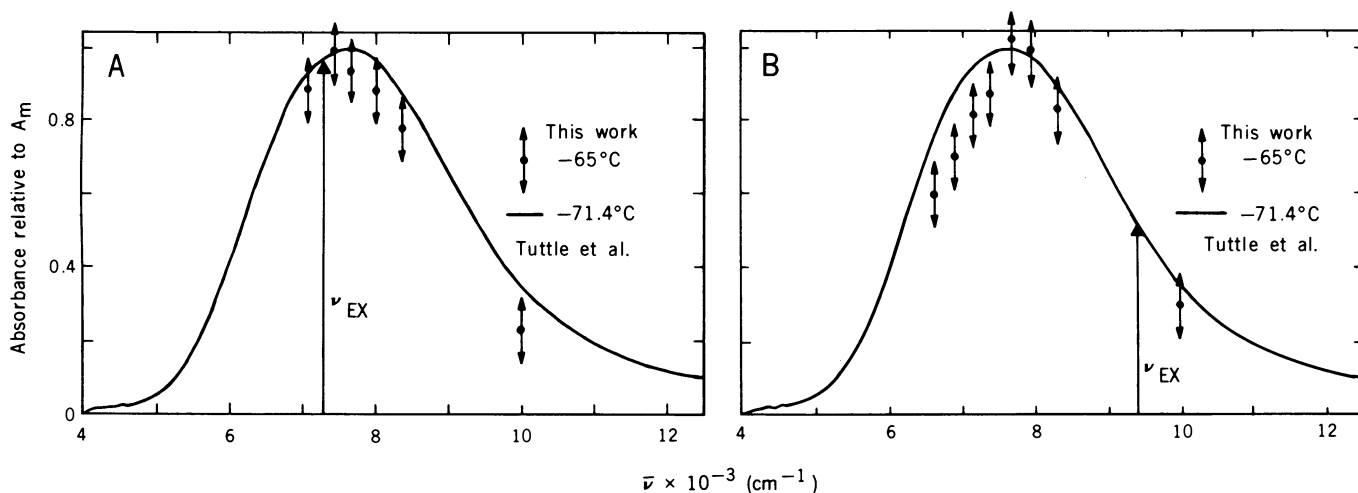


Fig. 6. Normalized absorbance change spectra of a Na-ND₃ solution at -65°C after excitation with a single 5-psec pulse. Interrogation was at the points indicated by double arrows, whose length is a measure of the reliability of the measurement. The solid line represents the steady-state absorption spectrum of the same system at -71.4°C (*46*). (A) Excitation at 7400 cm^{-1} (1060 nm). (B) Excitation at 9400 cm^{-1} (1350 nm).

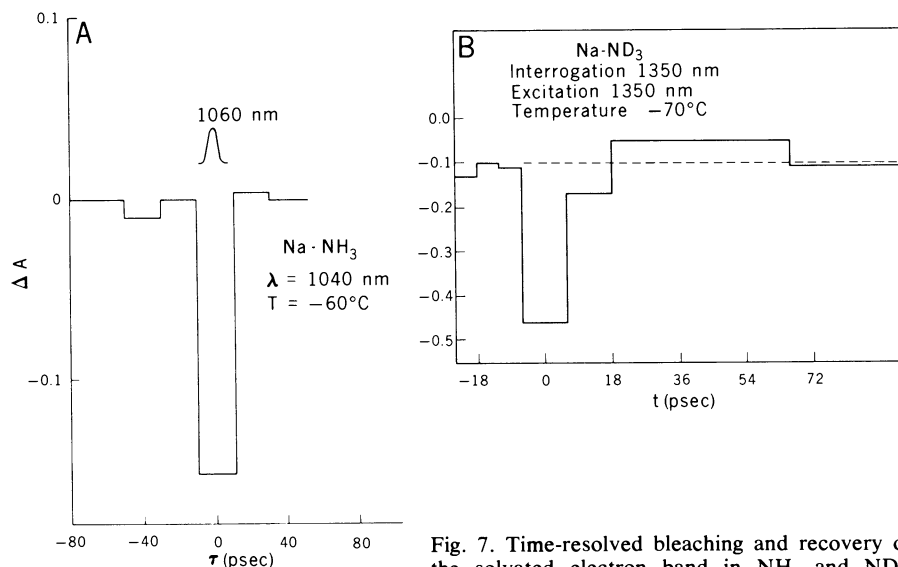


Fig. 7. Time-resolved bleaching and recovery of the solvated electron band in NH_3 and ND_3 . (A) The Na-NH_3 system excited by 1060-nm pulses and interrogated at 1040 nm with 20-psec time segments. (B) An Na-ND_3 sample excited by 1350-nm pulses and interrogated at 1350 nm with 12-psec time segments.

of pulses, each of which has a wavelength spread of 850 to 400 nm, a time width of 6 psec, and a separation from near neighbors of 10 psec.

Adjustment of the single excitation pulse to coincide in time and space in the sample cell with one of the early probe pulses allows the subsequent probe pulse to interrogate the events occurring picoseconds after excitation. To ensure accuracy, the probe pulse is split into two identical beams, I and I_0 , before entering the sample cell. Beam I_0 propagates through the air or a cell containing only the solvent, and for samples that easily deteriorate the reference beam, I_0 , monitors the absorbance just before the excitation pulse, I , interrogates absorbance

changes during and subsequent to excitation. The two beams are then passed into a spectrograph with their time dispersion axes resolved along the height of the slit. At the output of the spectrograph, a two-dimensional image is recorded with the time dispersion resolved along one axis and the wavelength resolved along the other. An example of a time-resolved spectrum is shown in Fig. 3, where the relaxation of a laser dye, DODCI (3,3'-diethyloxadicyanone iodide), is shown to depend on the power of the picosecond pulse and the concentration; this fact was not taken into consideration by some researchers, who did not realize the difference between the relaxation and emission lifetimes (30, 31).

Detection and Data Display

The histogram in Fig. 3 simultaneously portrays the spectroscopic and time events taking place from 650 to 540 nm and 6 to 80 psec, and it is laborious to extract and digitize all the information contained in this chronogram. The use of vidicon cameras has provided a significant improvement in linearity (10,000 for vidicons compared to ~ 10 for film) and sensitivity (an intensified vidicon can practically record single-photon events), as well as a great reduction in labor. Since the optical data are collected by the vidicon as electronic signals, the experimental results are ready for processing and display by an optical multi-channel analyzer in the form of intensity versus time (Fig. 4) or for direct input to an on-line computer. The amount of information recorded with a single shot can be extremely large. However, by employing a minicomputer it has become practical to process, analyze, and plot the data in brief periods of time, in a revealing and compact manner. Figure 5 shows a three-dimensional display of time (picoseconds), wavelength (nanometers), and intensity representing the events following the absorption of a picosecond pulse by a protein (32). This method has a sensitivity of 0.002 absorbance unit, time resolution limited by the width of the pulse, linear range of 10,000, reliability of ± 0.01 absorbance unit, and wavelength range and resolution strictly depending on the spectrometer. Data storage, averaging, and calculation of the average deviation are made routine by the use of the computer and double beam, as are the optical measurements

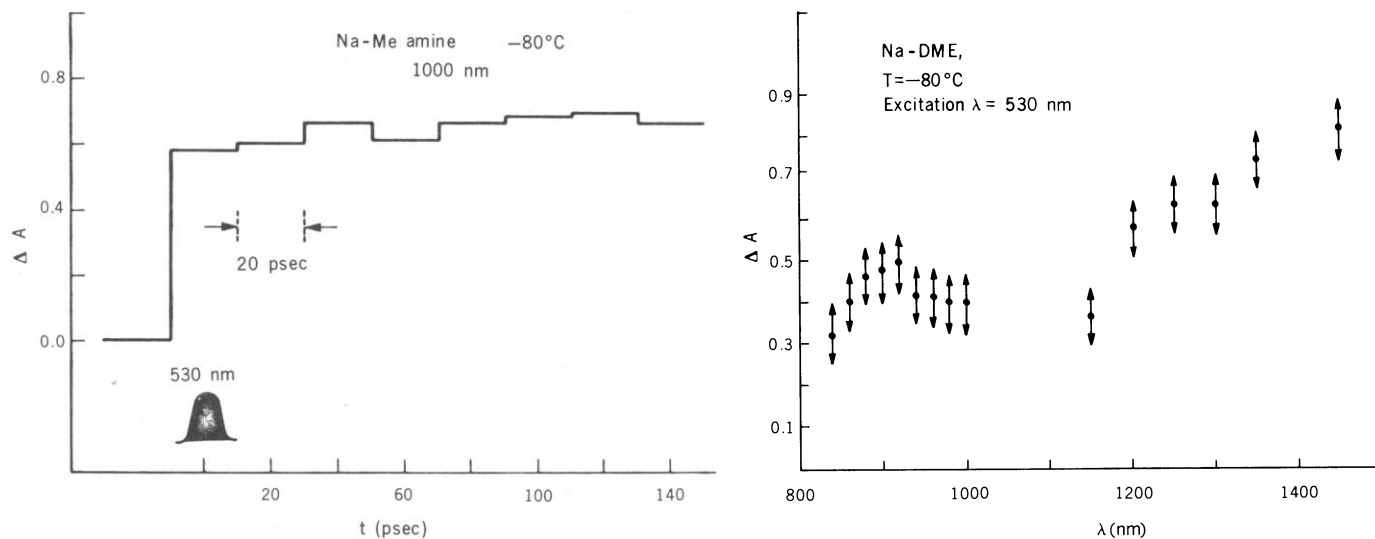


Fig. 8 (left). Formation dynamics of e^-_{solv} in an Na-methylamine solution at -80°C . Immediate formation of the e^-_{solv} band is observed after 530-nm picosecond excitation. Fig. 9 (right). Absorbance change spectrum observed after photoionization of NA^- in dimethoxyethane (DME) at -80°C with 530-nm pulses. The band with a maximum at ~ 900 nm is assigned to $(\text{Na}^+, e^-_{\text{solv}})$ species and the portion of the infrared band shown is due to e^-_{solv} .

of absorbance changes, decay lifetimes, light saturations, concentration dependence, and other parameters, which are often extremely difficult to measure without this method. Dual-beam picosecond absorption (16) spectroscopy with simultaneous detection of emission events by a streak camera is a powerful technique for studying picosecond and nanosecond events with the prototype system shown in Fig. 1.

Electrons in Fluids

The applications of picosecond spectroscopy cover a broad range and are increasing rapidly. The two studies selected for discussion in the rest of this article are only representative of the possibilities offered by this method.

The electron is the most basic particle in chemistry and biology. Electrons are responsible for the initial light absorption that causes photochemistry and initiates biological events such as the visual transduction process and photosynthesis. Therefore, knowledge of the behavior of electrons in chemical media and their rate of interaction with the media will provide some basis for deciphering the mechanisms of the initial events in photochemistry and biology.

Because of the reactivity of electrons, it is easier to study them in solutions of polar solvents and metals. The physical and optical properties of excess electrons from alkali metals dissolved in liquid ammonia have been extensively studied theoretically (33) by conventional techniques (34). However, picosecond spectroscopy (35) has provided additional information about (i) the mechanism of electron localization, (ii) the homogeneity of the solvated electron band and therefore about the structure and variety of "chemical species" involved in the process of solvolysis, (iii) the nature of excited states of the electron in fluids, (iv) the effect of the solvent, (v) relaxation processes, and possibly (vi) the photochemical properties of this species.

Picosecond studies of solvated electrons (e_{solv}^-) were performed in a cell having a 2-millimeter optical path length and containing a small amount of alkali metal (M) ($\sim 10^{-4}$ molar) in liquid ammonia. When the solvent is an amine or ether, not only solvated electrons but also alkaline anions and ion pairs of the type M^+ , e_{solv}^- appear. The absorption band of the solvated electron varies with solvents; however, in polar fluids and specifically in ammonia it is located in the near infrared with a maximum at ~ 1500 nm. There is a great deal of inter-

est in the absorption spectra of the solvated electron, the mode of relaxation of the excited state, and the detailed mechanism of the solvation (localization) process itself.

Since no emission has been observed from the excited state of e_{solv}^- , even though it was expected that the $2p \rightarrow 1s$

transition would be strongly allowed and would therefore have a radiative lifetime of $\sim 10^{-9}$ second, one is forced to conclude that a nonradiative mechanism must dominate the energy dissipation process. To study such processes ultrafast kinetic measurements are needed, and picosecond absorption spectroscopy

Fig. 10. Prelimirhodopsin difference spectrum 60 psec after excitation with a 5-mJ pulse at 530 nm: (○) 298 K, (●) 77 K, and (⊗) 4 K. The dotted curve is the photostationary difference spectrum at 77 K.

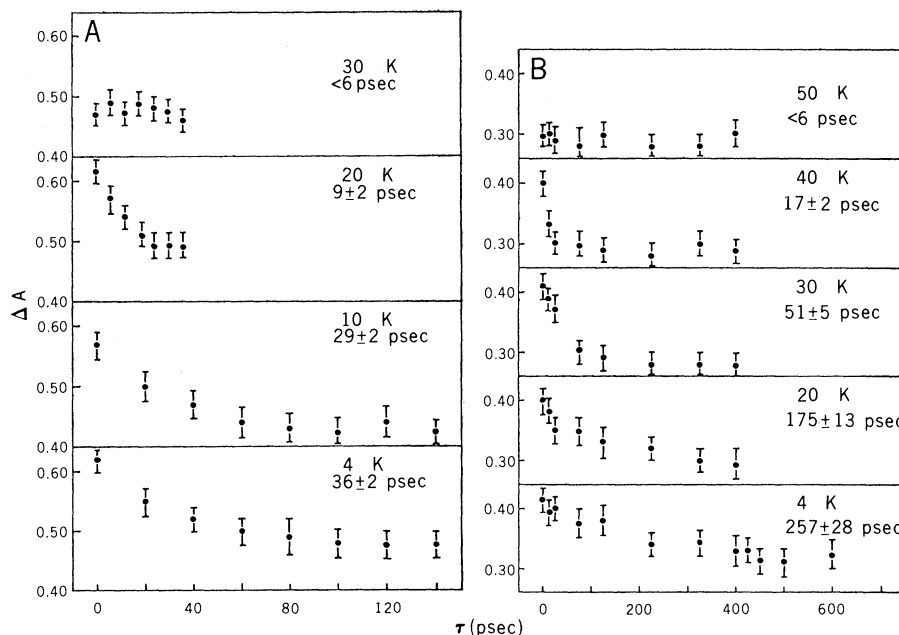
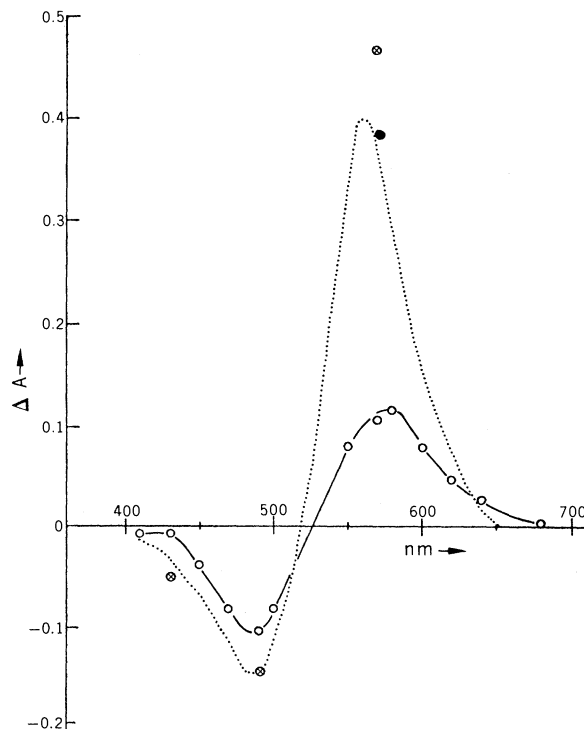


Fig. 11. (A) Formation kinetics of prelimirhodopsin between 30 and 4 K monitored at 570 nm. Rhodopsin was excited with 530-nm, 6-psec pulses. The low-temperature glass was formed by mixing one part of rhodopsin, solubilized in 0.3M Ammonyx and 0.01M Hepes at pH 7.0, with two parts of distilled ethylene glycol. The lifetime for formation, shown below the temperature in each panel, is the reciprocal of the rate constant obtained by a least-squares fit of a plot of $\ln(A_t - A_\infty)$ against time, t , in picoseconds, where A is the absorbance at 570 nm. (B) Same as (A) but the sample consisted of deuterium-exchanged rhodopsin. The low-temperature glass consisted of one part of deuterium-exchanged rhodopsin in deuterium-exchanged Ammonyx to two parts of deuterium-exchanged ethylene glycol.

provides the ideal tool. I will therefore present and analyze the optical picosecond data on the bleaching and repopulation of the ground state of e_{solv}^- in ammonia and amines with the expectation of gaining some insight into the nature, reactivity, and optical properties of e_{solv}^- .

The experiment was conducted with an experimental apparatus similar to that in Fig. 1. The excitation pulse was either a 1061-nm fundamental of the Nd^{3+} /glass, Nd^{3+} /YAG system or a 530-nm second harmonic or 1350-nm stimulated Stokes Raman pulse generated by focusing the 1061-nm pulse in a cell containing acetone. The interrogating beam consisted of a set of 12 broadband pulses, with the third or fourth pulse coincident with the excitation pulse in the cell. The two interrogating beams I and I_0 were imaged onto the slit of the spectrometer and its output was imaged on a vidicon target, which transmitted information to a computer for analysis and display on a graphics terminal.

Characteristics of the Solvated Electron

Absorption Band

The idea behind the experiment is simple. A laser pulse with a spectral width much narrower than the width of the steady-state absorption spectrum is used to bleach the absorption band of the solvated electron. If a hole (bleaching) is observed only at the same position of the spectrum as the spectral width of the excitation pulse, the spectrum is inhomogeneously broadened—that is, the electron absorption band is composed of a superposition of various species. However, if the laser pulse induces bleaching in the entire absorption band, or at least at wavelengths well outside its own spectral width, and if the bleaching follows the contour of the steady-state absorption band, then the band is homogeneous and composed of only one species.

Measurements were made on Na-NH_3 systems, using 1060-nm pulses ($\Delta\nu \sim 100 \text{ cm}^{-1}$, $\sim 6 \text{ psec}$, $\sim 30 \text{ mJ}$) for bleaching and a very weak continuum for probing in the spectral range 800 to 1100 nm (36). Because of the more favorable absorption cross section of e_{solv}^- in ND_3 , its properties were studied by bleaching at both 1060 and 1350 nm (7400 cm^{-1}) and the absorption changes were monitored between 800 and 1600 nm. Probing was performed within the time duration of the pulse and for several hundred picoseconds later. Figure 6, A and B, shows some of the changes taking place in the e_{solv}^- band in Na-ND_3 solution after excitation with 1350- and 1060-nm pulses.

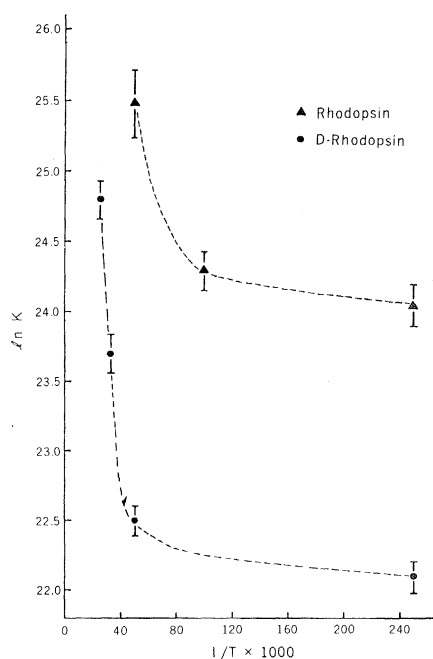


Fig. 12. Arrhenius plot of the data shown in Fig. 11; K is the formation rate of prelumirhodopsin; temperature, T , is in kelvins; and D-rhodopsin is deuterium-exchanged rhodopsin.

es. The solid lines in Fig. 6 show the steady-state absorption spectrum of e_{solv}^- in Na-ND_3 .

Figure 6 shows that the shape and intensity of the photoinduced bleaching of e_{solv}^- follows the steady-state absorption spectrum quite well. Analogous results were obtained for Na-NH_3 in the range 800 to 1100 nm. These results are interpreted to mean that the optical band of e_{solv}^- is homogeneous within the time and wavelength limits of the experiment. The possibility that the broad absorption band is the result of the superposition of different chemical species can be discarded, and the spectral width has to be assigned to a phonon broadening process or possibly to the unbound character of the excited state. It must be noted, however, that these observations cannot totally eliminate the case where the solvent cage engulfing the electron fluctuates considerably within the time period of the picosecond pulse. In such a system, different types of e_{solv}^- can be formed and the observed broad absorption can be attributed to variations in the coordination number and a wide spectrum of transition energies.

Repopulation and Excited State Dynamics of Solvated Electrons

To determine the dynamics of the ground state repopulation after electronic excitation, Na-NH_3 , Na-ND_3 , and

methylamine solutions were excited by a single 1060-nm or 1350-nm picosecond pulse. The recovery of the ground state absorption was monitored by using the picosecond continuum time-dispersed by the echelon to pulses with steps of 20, 13, or 7 psec (37). It was found that the bleaching and recovery of absorption occurred in a shorter period than any of these interrogating time intervals (Fig. 7, A and B). In addition, it was observed that the shape of interrogating pulse segments was symmetrical and identical before and after the bleaching. The absence of any observed distortion of the interrogating pulses indicates a much faster ground state repopulation than the time width of the pulse—in fact, more than an order of magnitude faster than the 7-psec monitoring time. The relaxation lifetime was calculated as 2×10^{-13} second from the absorbance changes, the absorption cross section, and the physical properties of the picosecond pulses. This subpicosecond lifetime was also found for Na-ND_3 , $\text{Na-dimethoxyethane}$, and other similar solutions.

Concerning the mechanism of the ultrafast relaxation of the excited state and repopulation of the ground state, the picosecond data do not support thermally induced photoionization involving activation to a higher electronic state (such as $2s$). However, ionization by a transition from a bound to an unbound state as well as a $2p \rightarrow 1s$ nonradiative transition may explain the data. A method that could, in principle, distinguish among these mechanisms would involve the solvation kinetics of a quasi-free electron. If the solvated electron was excited to an unbound state, it would be injected into the fluid to be solvated and would regenerate e_{solv}^- in the ground state. Therefore, the solvation rate and the ground state repopulation rate should be equal in this case.

The most convenient experimental systems for the study of quasi-free electrons are solutions of alkali metals in amines, particularly Na-methylamine , which exhibits a broad absorption band, assigned to Na^- , that has a maximum at 660 nm and extends below 500 nm. An experiment was performed in which the electron was generated by excitation with a 530-nm picosecond pulse and the resulting effect on Na^- was monitored by following absorbance changes between 590 and 650 nm. The kinetics of the solvation process was determined by probing the recovery of absorption of e_{solv}^- in methylamine in the range 770 to 1120 nm (38). It was found that although bleaching occurred within the 6-psec excitation pulse width, the Na^- absorption re-

mained practically unchanged for times longer than 200 psec. From the results shown in Fig. 8 it was determined that the e_{solv}^- absorption band achieves its maximum within the 6-psec duration of the pulse. The solvation lifetime was then calculated as $< 5 \times 10^{-12}$ second (38). It is important to note that no change was observed in this lower limit over the wide temperature range from room temperature to -100°C . This is particularly significant since the time for solvation of the electron in alcohols, measured by pulse radiolysis, is sensitive to temperature and is correlated with dielectric relaxation times.

These experiments suggest that (i) the absorption band of e_{solv}^- is homogeneously broadened, (ii) the broad e_{solv}^- band is not a superposition resulting from various chemical species, (iii) the asymmetric shape of the absorption band is due to phonon broadening, (iv) the subpicosecond relaxation or repopulation time, being similar in many solvents, is either the rate of the $2p \rightarrow 1s$ non-radiative transition or the rate of solvation of the quasi-free electron, and (v) the picosecond transient spectra (Fig. 9) of the cation-electron pair Na^+ , e_{solv}^- generated by the photoionization of Na^- can be obtained and analyzed.

Picosecond Phenomena in Vision

Study of the visual process is a natural application for picosecond spectroscopy. The process is activated by light in the visible region and undergoes consid-

erable change within very short periods of time. The goal of the picosecond studies has been to identify the kinetics and mechanism of formation of the species formed immediately after absorption of light by the visual chromophore rhodopsin.

It was already known that rhodopsin absorbs at 530 nm and, on light excitation, decays to the first intermediate, called prelumirhodopsin or bathorhodopsin, which has an absorption extending to 570 nm (39). Subsequently formed intermediates were identified as isomers of the original rhodopsin. It was therefore generally assumed that the only effect of the light was the isomerization of rhodopsin and that the first step in the visual process, the formation of prelumirhodopsin, was an isomerization process. There was speculation about the bond involved and the mechanism of isomerization.

The initial step in rhodopsin photochemistry was examined by picosecond spectroscopy in 1972 (40), and it was shown that the formation lifetime of the first intermediate was less than 6 psec (40, 41). This rate seemed too fast for the isomerization of a large molecule attached to a proton, and experiments were designed for an in-depth study of the initial events of rhodopsin photochemistry. The sample was made by solubilizing bovine retinal and was placed in a 2-mm cell that could be cooled to the temperature of liquid helium, 4 K. In an experimental setup similar to the one depicted in Fig. 1, the sample was excited at 530 nm and the subsequent absorption

changes were monitored from 440 to 700 nm; special care was given to the 570-nm region, which characterizes the prelumirhodopsin intermediate. It was made certain in every experiment that the pulse power did not produce nonlinear effects or saturation in the sample, but was kept in the linear range of absorbance change versus pulse power.

The absorbance changes observed after excitation for samples irradiated at room temperature (~ 300 K), 77 K, and 4 K are shown in Fig. 10 (40). Note that the amount of prelumirhodopsin intermediate does not decrease drastically as the temperature decreases, which would be expected for isomerization processes, but instead increases at 77 K by approximately a factor of 3.

Low-Temperature Kinetics

To elucidate the mechanism and identify the species involved in this primary process, the formation kinetics of prelumirhodopsin were monitored as a function of temperature. In addition, the sample was deuterated by exchange in D_2O and the effect of substituting deuterium for hydrogen was measured. The data obtained are shown in Fig. 11 (40). The lifetime for the formation of prelumirhodopsin continued to be less than 6 psec at temperatures as low as 30 K (Fig. 11A). Assuming isomerization as the prevailing mechanism, one would be forced to conclude that this large molecule isomerizes when frozen to 30 K at a rate higher than $1.5 \times 10^{11} \text{ sec}^{-1}$ and at

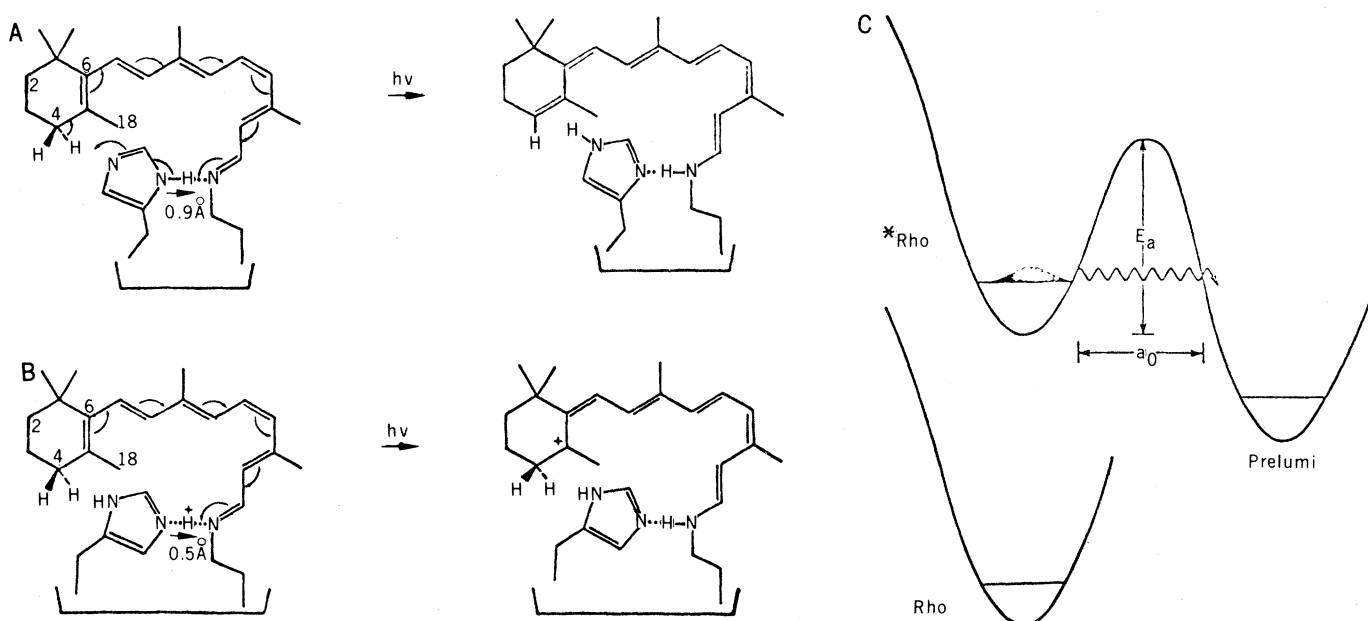


Fig. 13. Models proposed (40) for proton translocation to form prelumirhodopsin. (A) Single-proton translocation with carbonium ion formation. (B) Concerted double-proton translocation with retroretinal formation. (C) Tunneling potential energy barriers for formation of prelumirhodopsin; E_a represents the energy barrier and a_0 the translocation distance.

temperatures as low as 4 K at a rate of $2.5 \times 10^{12} \text{ sec}^{-1}$. Furthermore, since the hydrogens attached to the retinal skeleton, where isomerization takes place, do not exchange, one would expect deuteration to have a small or negligible effect on an isomerization process. However, when the experiment was repeated with D_2O -exchanged rhodopsin, the rate of formation of prelumirhodopsin decreased by a factor of 7 at 4 K (Fig. 11B). Even if the retinal protons were exchanged for deuterium (they were not in this experiment), the rate would not be lower by a factor of 7. When the rates of prelumirhodopsin formation are plotted in Arrhenius form ($\ln K$ versus $1/T$) the curves of Fig. 12 are obtained.

Proton Translocation

The data showed that we were unquestionably monitoring a proton translocation process that at low temperatures proceeds by a tunneling mechanism, with the proton tunneling through an activation barrier. From the rates obtained the height of the barrier was estimated to be ~ 0.7 kilocalorie and the proton translocation distance about 0.3 angstrom. Similar proton translocation was also observed in bacteriorhodopsin, but with a lower barrier (0.14 kcal). This work provided strong evidence that proton translocation is a primary event, if not the primary event, in vision. In addition, it provided direct kinetic evidence of proton tunneling, a phenomenon that is of major interest and has applications ranging from ferroelectrics to organic reactions.

It remains now to find out which proton moves. In one proposed model, illustrated in Fig. 13, it is the proton of the Schiff base retinal (40). Theoretical calculations (42) as well as spin resonance and other data (43) support this model. Other models based on our proton tunneling data, however, suggest that a proton of the protein is involved (44). At

present, there are no experimental data that unequivocally identify the proton that is translocated. However, there is widespread acceptance, even among the strongest supporters of the isomerization mechanism, which is involved in some intermediate states, that the proton transfer mechanism shown by picosecond spectroscopy is a primary event in the visual transduction process.

Many other chemical, physical, and biological phenomena have been or are being studied by picosecond spectroscopy, including photosynthesis, semiconduction, organic reactions, and ferroelectricity. In the near future, one can foresee even shorter pulses with high photon fluxes tunable from the vacuum ultraviolet to the infrared region of the spectrum. Picosecond resonance Raman experiments are already being done, and picosecond spectroscopy should become as useful as conventional ultraviolet, infrared, and Raman spectroscopy with the added dimension of time resolution.

References and Notes

1. P. M. Rentzepis, *Chem. Phys. Lett.* **2**, 37 (1968).
2. R. R. Alfano and S. L. Shapiro, *ibid.* **8**, 231 (1971); D. Von der Linde, D. Meier, W. Kaiser, *Phys. Rev.* **178**, 11 (1969).
3. J. Jortner and R. S. Berry, *J. Chem. Phys.* **48**, 2757 (1968).
4. W. S. Struve, *Proc. Eur. Spectrosc. Symp.*, in press.
5. R. Levin and J. Jortner, Eds., *Molecular Energy Transfer* (Wiley, New York, 1976).
6. K. J. Kaufmann and P. M. Rentzepis, *Acc. Chem. Res.* **8**, 407 (1975).
7. K. B. Eisenthal, *ibid.*, p. 118.
8. P. Avouris, K. S. Peters, P. M. Rentzepis, *Biophys. J.* **21**, 8a (1978).
9. J. Jortner and N. R. Kestner, Eds. *Electrons in Fluids* (Springer-Verlag, Berlin, 1973).
10. K. J. Kaufmann, P. L. Dutton, T. L. Netzel, J. S. Leigh, P. M. Rentzepis, *Science* **188**, 1301 (1975).
11. G. Porter, J. A. Synowiec, C. J. Tredwell, *Biochim. Biophys. Acta* **459**, 329 (1977).
12. M. G. Rockley, M. W. Windsor, R. J. Cogdell, W. W. Parson, *Proc. Natl. Acad. Sci. U.S.A.* **72**, 2251 (1975).
13. J. A. Giordmaine, P. M. Rentzepis, S. L. Shapiro, K. Wecht, *Appl. Phys. Lett.* **11**, 216 (1967); P. M. Rentzepis and M. A. Duguay, *ibid.*, p. 218.
14. P. M. Rentzepis, C. J. Mitschele, A. C. Saxman, *ibid.* **17**, 112 (1970).
15. D. J. Bradley and W. Sibbert, *Opt. Commun.* **9**, 17 (1973); D. J. Bradley and G. H. L. New, *Proc. IEEE* **63**, 313 (1974).
16. T. L. Netzel and P. M. Rentzepis, *Chem. Phys. Lett.* **29**, 337 (1974).
17. F. O. O'Neil, *Opt. Commun.* **6**, 360 (1970); E. P. Ippen, C. V. Shank, A. Dienes, *Appl. Phys. Lett.* **21**, 348 (1972); D. J. Bradley, *ibid.* **20**, 125 (1972).
18. E. P. Ippen, C. V. Shank, A. Lewis, M. A. Marcus, *Science* **200**, 1279 (1978).
19. C. V. Shank, E. P. Ippen, R. Bersohn, *ibid.* **193**, 50 (1975).
20. E. P. Ippen, C. V. Shank, R. L. Woerner, *Chem. Phys. Lett.* **45**, 291 (1977).
21. D. Huppert and P. M. Rentzepis, *Appl. Phys. Lett.* **32**, 211 (1978).
22. ———, *J. Appl. Phys.* **49**, 543 (1978).
23. E. R. Zavoiskii and S. S. Franchenko, *Sov. Phys. Dokl.* **1**, 285 (1956).
24. G. Porter, *Bakerian Lecture* (Royal Society, London, 1977); L. Rubin and A. Rubin, *Biophys. J.*, in press.
25. G. R. Flemming, A. E. W. Knight, J. M. Morris, R. J. S. Morrison, G. W. Robinson, *J. Am. Chem. Soc.* **99**, 4306 (1977); K. K. Smith, J. Y. Koo, G. B. Schuster, K. J. Kaufmann, *Chem. Phys. Lett.* **48**, 267 (1977).
26. D. J. Bradley and W. Sibbert, *Appl. Phys. Lett.* **27**, 382 (1975).
27. R. R. Alfano and S. L. Shapiro, *Phys. Rev. Lett.* **24**, 534 (1969).
28. G. E. Busch and P. M. Rentzepis, *Chem. Phys. Lett.* **18**, 178 (1973).
29. M. R. Topp and P. M. Rentzepis, *Chem. Phys.* **4**, 1 (1971); *J. Appl. Phys.* **42**, 3451 (1971).
30. C. V. Shank and E. P. Ippen, *Appl. Phys. Lett.* **26**, 62 (1975).
31. D. Magde and M. W. Windsor, *Chem. Phys. Lett.* **27**, 31 (1974).
32. D. Huppert, K. D. Straub, P. M. Rentzepis, *Proc. Natl. Acad. Sci. U.S.A.* **74**, 4139 (1977).
33. D. N. Kestner and J. Jortner, *J. Phys. Chem.* **77**, 1040 (1973); J. J. Lagowski and M. J. Sienko, Eds., *Metal-Ammonia Solutions* (Butterworth, London, 1970).
34. B. Bockrath and L. M. Dorfman, *J. Phys. Chem.* **77**, 1002 (1973).
35. P. M. Rentzepis, R. P. Jones, J. Jortner, *Chem. Phys. Lett.* **15**, 480 (1972).
36. D. Huppert, W. S. Struve, P. M. Rentzepis, J. Jortner, *J. Chem. Phys.* **64**, 195 (1976).
37. D. Huppert, P. Avouris, P. M. Rentzepis, *J. Phys. Chem.*, in press.
38. D. Huppert and P. M. Rentzepis, *J. Chem. Phys.* **64**, 195 (1976).
39. T. Yoshizawa and G. Wald, *Nature (London)* **197**, 1279 (1963).
40. G. E. Busch, M. L. Applebury, A. A. Lamola, P. M. Rentzepis, *Proc. Natl. Acad. Sci. U.S.A.* **69**, 2802 (1972).
41. V. Sundstrom, P. M. Rentzepis, K. S. Peters, M. L. Applebury, *Nature (London)* **267**, 645 (1977).
42. L. Salem and D. Bruckmann, *ibid.* **258**, 526 (1975).
43. R. Mathies and L. Stryer, *Proc. Natl. Acad. Sci. U.S.A.* **73**, 2169 (1976).
44. A. Lewis, *ibid.* **75**, 2 (1978).
45. L. J. Noe, W. G. Eisert, P. M. Rentzepis, *ibid.*, p. 573.
46. I. Hurley, T. R. Tuttle, J. Golend, in *International Conference on the Nature of Metal-Ammonia Solutions*, J. J. Lagowski and M. J. Sienko, Eds. (Butterworth, London, 1970).
47. The work presented has been the product of collaboration with M. L. Applebury, G. E. Busch, A. A. Lamola, and K. S. Peters in vision; D. Huppert, K. J. Kaufmann, T. L. Netzel, L. J. Noe, and W. S. Struve in the development of most experimental aspects; D. Huppert, J. Jortner, and W. S. Struve in work on solvated electrons; and D. C. Douglass throughout all aspects.